ChemComm

COMMUNICATION

View Article Online
View Journal

Cite this: DOI: 10.1039/d6cc00868b

Received 9th February 2026,
Accepted 2nd April 2026

DOI: 10.1039/d6cc00868b

rsc.li/chemcomm

Desaturative arylaldehyde synthesis by synergistic carbocatalysis and organocatalysis

Naokatsu Kannari,*[ab] Ivan Curic,[b] Nina Place,[b] Lukas Enders,[b] Shotaro Kawasaki,[a] Anna Lenarda *[b] and Juho Helaja *[b]

A metal-free cooperative carbocatalyst–organocatalyst system promotes the dehydrogenative aromatization of 3-cyclohexene aldehydes to aromatic aldehydes. Quinone-rich, oxidized activated carbon and secondary amines act synergistically, providing a structurally diverse substrate scope. Mechanistic studies indicate a predominantly ionic hydride-transfer pathway and identify pore-blocking as the main cause of catalyst deactivation.

Carbon materials are widely employed as supports for metal catalysts owing to their thermal robustness, chemical stability, and high surface areas. Beyond this role, appropriately engineered carbons can display intrinsic catalytic activity, particularly when modified through heteroatom doping.[1–3] These materials, termed carbocatalysts, have emerged as sustainable and cost-effective alternatives to metal-based systems. Their activity is commonly associated with structural defects and heteroatom-containing functional groups at graphitic edges. Quinone-type moieties have been reported to play a central role in several oxidative dehydrogenation (ODH) processes ranging from industrial production of commodity chemicals[4] (*e.g.* styrene from ethylbenzene) to liquid-phase coupling and aromatization reactions.[1,5–7]

Our group has previously developed oxygen-rich carbon materials for the ODH aromatization of unsaturated carbocycles and carboheterocycles to access (hetero)aryls[6,7] and heterobiaryls.[8]

Aromatic aldehydes constitute a high-value class of compounds used extensively in pharmaceuticals, agrochemicals, fragrances, and fine chemicals.[9] Conventional synthetic routes often rely on stoichiometric oxidants or precious metals, motivating the development of greener alternatives.[10]

Catalytic dehydrogenative aromatization represents a distinct desaturative approach in which redox-active enamines, generated from non-aromatic precursors, undergo sequential oxidation and dehydrogenation to afford functionalized arenes.[11] In this context, Leonori and co-workers introduced a dual photoredox-cobalt catalytic method approach for the synthesis of anilines from cyclohexanone and amine building blocks.[12] This work enabled the development of related enamine-aromatization approaches to aryl amines under electro-[13] photo[14] and Pd-[15] catalysis conditions.

Building on this concept Lenarda *et al.*[16] recently reported a carbocatalyzed condensation–oxidative aromatization cascade affording diarylamines from partially unsaturated cyclic ketones, demonstrating cooperative metal-free redox activity of quinones and other oxygenated surface functionalities on porous carbon.

Leonori *et al.* subsequently extended enamine-mediated desaturation to aldehydes trough a triple catalytic system combining Ir-based photoredox catalysis, organocatalytic enamine activation, and cobalt co-catalysis.[17] In this system, enamine formation with a secondary amine (*e.g.*, morpholine) enables single electron transfer (SET) oxidation followed by hydrogen atom transfer (HAT) dehydrogenation, mediated, respectively, by the photoredox and cobalt catalysts (Fig. 1).

Guided by this insight, we envisioned that quinone-rich oxidized carbon materials could, in combination with a secondary amine co-catalyst, promote the ODH step of this reaction. We therefore initiated our study using HNO_3-oxidized activated carbon (oAC_{HNO_3}), prepared from commercial activated carbon (AC) following a protocol established in our laboratory,[6] as the carbocatalyst. X-ray photoelectron spectroscopy (XPS) and temperature-programmed desorption (TPD) analyses confirmed the presence of abundant oxygenated functionalities, including quinone moieties, in agreement with previous reports (Fig. S1, S2, and Tables S1, S2), on a 635 $m^2\ g^{-1}$ surface area characterized by an extended porous network (Table S9).[6]

At first, we evaluated different secondary amines as organo-*co*-catalysts using the dehydrogenative aromatization of Cyclohex-3-ene-1-carbaldehyde (**1a**) as a probe reaction, in conditions previously optimized for oAC catalyzed ODH aromatization reactions.[6]

[a] *Division of Materials and Environment, Graduate School of Science and Technology, Gunma University, 1-5-1, Tenjin-cho, Kiryu, Gunma 376-8515, Japan. E-mail: nkannari@gunma-u.ac.jp*

[b] *Department of Chemistry, University of Helsinki, A. I. Virtasen aukio 1, P.O. Box 55, Helsinki 00014, Finland. E-mail: anna.lenarda@helsinki.fi, juho.helaja@helsinki.fi*

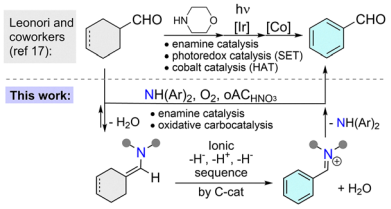

Fig. 1 Dehydrogenative aromatization cascades of aldehydes utilizing enamine, Ir-photoredox, and cobalt *vs.* quinone-based redox carbocatalysis with proposed mechanism for the amine-mediated step.

Morpholine (**A1**), previously employed in photoredox-mediated cyclohexene dehydrogenation,[17] afforded only a marginal yield increase of 5% relative to the amine-free control (Table 1, entries 3 and 4), and phenoxazine (**A2**) and phenothiazine (**A3**) were similarly ineffective. In contrast, diphenylamine-derived catalysts showed markedly higher activity, with diphenylamine (**A4**), bis(4-methylphenyl)amine (**A5**), and bis(4-methoxyphenyl)amine (**A6**) delivering progressively higher yields, of 37%, 47% and 70% respectively. This trend suggests an enamine-mediated activation pathway in which more electron-rich diarylamines generate enamines better matched to the redox properties of the quinone sites on oAC_{HNO3} (Fig. 1).

After optimization of the reaction conditions (Table S4), the influence of AC surface oxidation on catalytic performance was examined using **A6** as the amine co-catalyst (Table 1). HNO_3-oxidized activated carbon (oAC_{HNO3}) afforded high aromatization efficiency (70% yield), whereas AC_{dm} and untreated AC showed markedly lower activity (entries 9 and 10). This enhancement is consistent with the increased concentration of quinone-type functionalities introduced by nitric acid oxidation. Notably, untreated ACs retained moderate activity, likely due to native quinone groups inherently present in commercial activated carbons.[18]

Table 1 Catalyst and co catalyst screening

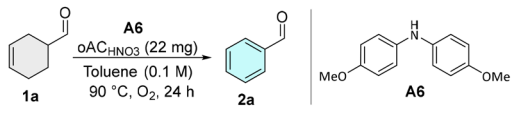

Entry	Variation of reaction conditions	Yield of **2a** (%)	Conversion of **1a** (%)
1	**None**	**70**	**90**
2	no oAC_{HNO3}, **A6**	0	4
3	oAC_{HNO3}, **no A6**	2	56
4	**A1** (morpholine) instead of **A6**	5	51
5	**A2** (phenoxazine) instead of **A6**	3	34
6	**A3** (phenothiazine) instead of **A6**	4	38
7	**A4** (diphenylamine) instead of **A6**	37	60
8	**A5** (bis(4-methylphenyl)amine) instead of **A6**	47	69
9	AC_{dm} as catalyst	51	63
10	AC as catalyst	29	38
11	HT-oAC_{HNO3} as catalyst	14	43
12	HT-AC_{dm} as catalyst	9	23
13	Anthraquinone (0.5 equiv.) as catalyst	2	6
14	PQ (0.5 equiv.) as catalyst	7	17

Thermal removal of oxygen functionalities by high-temperature treatment (HT-AC_{dm} and HT-oAC_{HNO3}, entries 11 and 12) led to a pronounced loss of activity, corroborating the essential role of oxygenated active sites. In particular, XPS O1s deconvolution reveals a clear correlation between C=O content and product yield (Fig. 2), suggesting the critical role of these functionalities in the catalytic process. In contrast, molecular quinones displayed only modest catalytic activity (entries 13 and 14), with 0.5 equiv. of 9,10-phenanthrenequinone (PQ) affording a remarkably low yield of 7%, only slightly higher than the one obtain in absence of catalyst (entry 2). These results suggest that efficient catalysis requires not only functional redox centres but also the presence of an extended, porous carbon framework, which appears to play a crucial electronic and structural role.

While the correlation presented in Fig. 2 suggests that quinone sites on the carbon play a crucial role in the catalytic activity, it is acknowledged that XPS peak deconvolution inherently involves overlapping components. Therefore, The role of different functional groups as the catalytically active sites was further probed through selective surface-group blocking experiments, using previously reported procedures (Fig. S3).[16] Blocking –OH and –COOH groups had a negligible effect on catalytic performance, affording product yields of 70% and 68%, respectively, comparable to that obtained with untreated oAC_{HNO3} (70%). In contrast, selective masking of carbonyl groups led to a sharp decrease in activity, with the yield dropping to 20%. XPS analysis confirmed the selective modification of the targeted oxygen functionalities (Fig. 2 and Tables S5, S6, Fig. S4). These results provide further substance to our hypothesis of quinone groups being the active sites responsible for dehydrogenative aromatization catalysis.

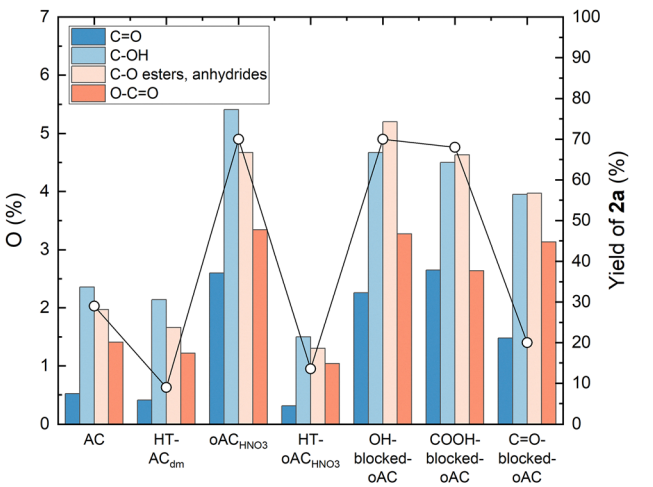

Fig. 2 Atomic percentages from XPS O1s spectra (bars) and yields % of **2a** (line with circles). AC, HT-AC_{dm}, oAC_{HNO3} and HT-oAC_{HNO3} represent pristine, demineralized/heat-treated (1000 °C), HNO_3-oxidized and HNO_3-oxidized/heat-treated (1000 °C) ACs, respectively. OH–, COOH– and C=O-blocked-oAC represent oAC_{HNO3} with their respective functional groups blocked.

With the catalytic system established, we next examined the substrate scope for the dehydrogenative aromatization of cyclohexene aldehydes (Fig. 3). Yields are reported as isolated unless otherwise stated, subject to purification constraints. Under the standard conditions (toluene, 90 °C), 2,4-dimethylcyclohex-3-ene-1-carbaldehyde (**2b**) afforded the aromatic aldehyde in 36% yield after 24 h, indicating modest steric inhibition relative to **1a**. In contrast, aryl-fused substrates were efficiently converted: the biphenyl-derived aldehyde **2c** was obtained in 89% yield after 48 h, while a naphthyl analogue **2d** furnished 79% yield under identical conditions. Both electron-withdrawing and electron-donating substituents were tolerated, with 4′-CF_3 (77%, **2e**), 3′,4′-dimethoxy (89%, **2f**), and 3′,5′-dimethyl (49% after 72 h, **2g**) derivatives providing the corresponding aldehydes. Strongly electron-donating substituents led to diminished performance, as observed for the 4′-dimethylamino substrate (49%, **2h**). A heteroaromatic thiophene-containing substrate was also proved compatible, affording 4-(thiophen-3-yl)benzaldehyde **2i** in 53% yield. Overall, the reaction tolerates a broad range of electronic environments, with highest efficiency observed for biphenyl-derived systems, consistent with an enamine oxidation pathway modulated by substrate electronics.

The durability of the carbocatalyst was evaluated through recycling experiments using **1a** as a model substrate. Activity progressively decreased over successive cycles, indicating catalyst deactivation (Fig. S5a). Amine recovery experiments showed significant retention of the secondary amine on the catalyst, suggesting surface adsorption as a primary deactivation pathway (Fig. S5b). Consistently, N_2 physisorption revealed loss of surface area and microporosity upon reuse (Fig. S7 and Table S9), consistent with pore blocking by adsorbed amines.

Post-reaction XPS analysis showed no significant changes in overall surface composition were observed, although a slight decrease in the C═O content was detected (Tables S7 and S8).

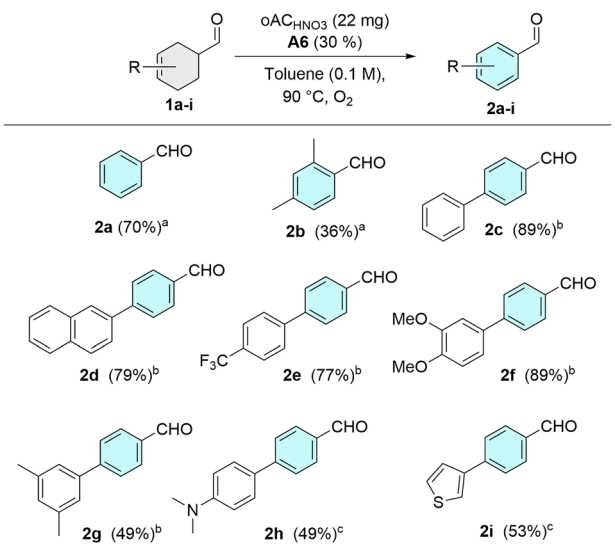

Fig. 3 [a]24 h, GC yield, [b]48 h, isolated yield, [c]48 h, NMR yield. Scope study for the aromatization of cyclohexene-3-aldehydes.

Combined with the BET data, these results are consistent with reversible deactivation *via* adsorption of amine species on active sites and within the porous structure.

Importantly, catalyst deactivation was found to be reversible; washing the spent material with acetic acid restores catalytic activity and textural properties close of the fresh catalyst (Fig. S6 and Table S7). These indicates that deactivation primarily arises from reversible amine adsorption, which blocks quinone active sites and the porous carbon framework.

Additional evidence for pore-blocking-induced deactivation was obtained from catalytic tests in the presence of pyrene, employed as an inert polycyclic aromatic probe to occupy pore volume. Consistent with prior reports,[16] pyrene was selected for its strong π–π affinity for carbon surfaces and its ability to physically reside within micropores without participating in the reaction. The addition of two equivalents of pyrene reduced the yield to 53%, consistent with progressive pore occupation limiting access of the substrate, intermediates, and organocatalyst. Similar experiments performed under Ar in presence of non-aromatic probes resulted in lowered yields (see SI).

The critical role of porosity was further supported by experiment using reduced graphene oxide (rGO), a commonly reported carbocatalyst for oxidative dehydrogenation.[3,16] Despite its high oxygen content, rGO afforded only 1% yield under the optimized conditions, indicating that surface oxygen functionalities alone are insufficient for efficient catalysis (see SI). Together with the pyrene-blocking and recycling studies, these results suggest pore accessibility as critical for catalytic activity.

Collectively, these results indicate that quinone active sites and an accessible porous carbon framework must operate cooperatively to enable efficient enamine oxidation and aromatization.

PQ is frequently employed as a molecular model for quinone-mediated dehydrogenative carbocatalysis on oxidized carbon materials.[19]

To gain theoretical insight, DFT calculations were performed on the dehydrogenative aromatization of enamines **1a-A4** and **1a-A6** mediated by PQ (Table S11 and Fig. S8). The reaction proceeds *via* an initial hydride abstraction from the doubly allylic C2 position, followed by deprotonation and a second hydride abstraction to afford the aromatic aldehyde. However, the computed barriers for the first hydride abstraction are relatively high (30.0 and 29.0 kcal mol^{-1}), indicating that PQ alone does not fully capture the experimentally observed reactivity of oAC_{HNO3}.

To refine the model and better account for the extended π-conjugation effects, coronenequinone (CQ) was next examined (Table S12 and Fig. S10). Although the reaction mechanism remains unchanged, the larger π-system lowers the initial activation barriers to 24.5 and 21.7 kcal mol^{-1}. Incorporation of a carboxylic acid group onto CQ (CQCA), mimicking nitric acid–oxidized carbon, further reduces these values to 23.6 and 19.9 kcal mol^{-1} (Fig. 4), and accurately reproduces the experimental enamine reactivity trend. Notably, the CO_2H substituent acts as an electron withdrawing group, rendering the π-surface

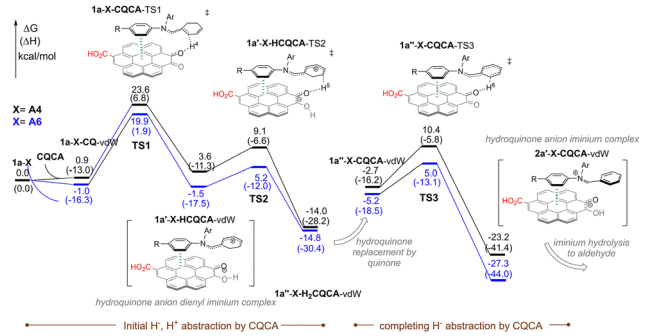

Fig. 4 Gibbs free-energy profiles for CQCA-mediated aromatization of enamines **1a**-**A4** and **1a**-**A6**. M06-2X/6-311++G(d,p)//M06-2X/6-31+G(d,p), CPCM(toluene), GD3.

of CACQ more electron-deficient and thereby strengthening its interaction with the enamine.

Noncovalent interaction (NCI) analysis reveals stabilizing π–π interactions between the enamine and the CQ–CO_2H surface, while HOMO analysis indicates greater delocalization for the more reactive **1a-A6** system (see SI, NCI plots section). Moreover, DFT calculations predict that the morpholine-derived enamine (**1a-Morp**) is similarly reactive to **1a-A4** (Fig. S9 and S11); its poor experimental performance likely arises from inefficient enamine formation under the acidic oAC_{HNO_3} carbocatalyst conditions. This interpretation is supported by its strong H-bonding interaction with the CO_2H site of model compound CACQ (see Fig. S12 and Table S15).

Although TEMPO-like radical traps substantially suppress reactivity (Table S10), computational analysis shows that SET and HAT pathways between enamines and quinone models are thermodynamically unfavourable (Tables S13 and S14), suggesting a predominantly ionic hydride-transfer mechanism,[20] with radical species contributing only to catalyst regeneration, as supported by the moderate yield obtained in the tests performed under Ar atmosphere (see Table S4).[21] Nevertheless, based on computations with model compounds alone, a radical component in the catalytic cycle cannot be fully excluded.

In summary, we report a metal-free, cooperative carbocatalyst–organocatalyst strategy for the dehydrogenative aromatization of cyclohexene aldehydes to aromatic aldehydes under mild conditions. Quinone-rich oxidized activated carbon acts as the redox-active catalyst, while secondary amines enable formation of reactive enamine intermediates. The method displays a diverse substrate scope, efficiently converting aryl-fused, biphenyl-derived, heteroaromatic cyclohexene aldehydes bearing both electron-donating and electron-withdrawing substituent. Experimental and computational studies suggest quinone surface sites and carbon porosity as key determinants of activity, with catalyst deactivation likely arising from reversible pore blocking by amines. Mechanistic investigations support a predominant ionic hydride-transfer pathway. Overall, this work expands the scope of carbocatalysis and underscores the potential cooperative catalyst design in sustainable oxidation chemistry.

N. K.: writing – original draft preparation, conceptualization, investigation (catalyst development and catalyst testing), analysis of results, resources and funding acquisition, I. C.: investigation (synthetic work and catalyst testing), N. P.: investigation (synthetic work), L. E.: investigation, methodology (synthetic work), S. K.: investigation (TPD measurement), A. L.: methodology (catalysis testing), analysis of results, writing – review and editing, visualization, J. H.: investigation (DFT calculation), writing – review and editing, project administration, resources and funding acquisition.

Conflicts of interest

There are no conflicts to declare.

Data availability

All data supporting the findings of this study are available within the article and its supplementary information (SI). Supplementary information: additional catalytic experiments; synthetic procedures; product characterization (NMR including copies of relevant spectra); additional XPS; BET data and spectra; computational details; XYZ parameters. See DOI: https://doi.org/10.1039/d6cc00868b.

Acknowledgements

This study was supported in part by the Uehara Memorial Foundation, the Scandinavia-Japan Sasakawa Foundation, and the Kondo Memorial Foundation. Financial support from the Academy of Finland [project no. 356338 (J. H.)] is acknowledged. The Finnish National Centre for Scientific Computing (CSC) is recognized for computational resources. XPS measurements were performed at the Core Facility Management and Technical Collaboration Center (CoMTeCC) of Gunma University.

References

1 (*a*) D. S. Su, G. Wen, S. Wu, F. Peng and R. Schlögl, *Angew. Chem., Int. Ed.*, 2017, **56**, 936–964; (*b*) D. R. Dreyer and C. W. Bielawski, *Chem. Sci.*, 2011, **2**, 1233–1240; (*c*) D. R. Dreyer, A. D. Todd and C. W. Bielawski, *Chem. Soc. Rev.*, 2014, **43**, 5288–5301; (*d*) H. Jia, D. R. Dreyer and C. W. Bielawski, *Tetrahedron*, 2011, **67**, 4431; (*e*) D. R. Dreyer, H. Jia and C. W. Bielawski, *Angew. Chem., Int. Ed.*, 2010, **49**, 6813; (*f*) P. Tang, G. Hu, M. Li and D. Ma, *ACS Catal.*, 2016, **6**, 6948–6958; (*g*) M. S. Ahmadab and Y. Nishina, *Nanoscale*, 2020, **12**, 12210–12227; (*h*) D. S. Su, J. Zhang, B. Frank, A. Thomas, X. Wang, J. Paraknowitsch and R. Schlögl, *ChemSusChem*, 2010, **3**, 169–180.

2 (*a*) D. Yu, E. Nagelli, F. Du and L. Dai, *J. Phys. Chem. Lett.*, 2010, **1**, 2165–2173; (*b*) J. Zhang, D. Su, A. Zhang, D. Wang, R. Schlögl and C. Hébert, *Angew. Chem., Int. Ed.*, 2007, **46**, 7319–7323; (*c*) D. S. Su, S. Perathoner and G. Centi, *Chem. Rev.*, 2013, **113**, 5782–5816; (*d*) R. P. Rocha and J. L. Figueiredo, *Catalysts*, 2025, **15**, 443; (*e*) S. Navalon, A. Dhakshinamoorthy, M. Alvaro, M. Antonietti and H. García, *Chem. Rev.*, 2017, **46**, 4501–4529; (*f*) J. Zhou, P. Yang, P. A. Kots, M. Cohen, Y. Chen, C. M. Quinn, M. D. de Mello, J. Anibal Boscoboinik, W. J. Shaw, S. Caratzoulas, W. Zheng and D. G. Vlachos, *Nat. Commun.*, 2023, **14**, 2293.

3 (*a*) S. Navalon, A. Dhakshinamoorthy, M. Alvaro and H. Garcia, *Chem. Rev.*, 2014, **114**, 6179–6212; (*b*) S. C. Wu, L. H. Yu, G. D. Wen, Z. L. Xie and Y. M. Lin, *J. Energy Chem.*, 2021, **58**, 318–335.

4 J. Zhang, X. Liu, R. Blume, A. Zhang, R. Schlögl and D. S. Su, *Science*, 2008, **322**, 73–77.
5 (*a*) D. S. Casadio, S. Aikonen, A. Lenarda, M. Nieger, T. Hu, S. Taubert, D. Sundholm, M. Muuronen, T. Wirtanen and J. Helaja, *Chem. – Eur. J.*, 2021, **27**, 5283–5291; (*b*) T. Wirtanen, S. Aikonen, M. Muuronen, M. Melchionna, M. Kemell, F. Davodi, T. Kallio, T. Hu and J. Helaja, *Chem. – Eur. J.*, 2019, **25**, 12288–12293; (*c*) T. Wirtanen, M. K. Mäkelä, J. Sarfraz, P. Ihalainen, S. Hietala, M. Melchionna and J. Helaja, *Adv. Synth. Catal.*, 2015, **357**, 3718–3726; (*d*) A. Lenarda, T. Wirtanen and J. Helaja, *Synthesis*, 2023, 45–61; (*e*) S. Wu, L. Yu, G. Wen, Z. Xie and Y. Lin, *J. Energy Chem.*, 2021, **58**, 318–335; (*f*) H. Jung and C. W. Bielawski, *RSC Adv.*, 2020, **10**, 15598–15603; (*g*) H. Jia, D. R. Dreyer and C. W. Bielawski, *Adv. Synth. Catal.*, 2011, **353**, 528; (*h*) W. Qi and D. Su, *ACS Catal.*, 2014, **4**, 3212–3218.
6 L. Enders, D. S. Casadio, S. Aikonen, A. Lenarda, T. Wirtanen, T. Hu, S. Hietala, L. S. Ribeiro, M. F. R. Pereira and J. Helaja, *Catal. Sci. Technol.*, 2021, **11**, 5962–5972.
7 A. Lenarda, M. Melchionna, S. Aikonen, T. Montini, P. Fornasiero, T. Hu, M. Hummel and J. Helaja, *ACS Catal.*, 2023, **13**, 11362–11375.
8 M. Yang, A. Lenarda, S. Frindy, Y. Sang, V. Oksanen, A. Bolognani, L. Hendrickx, J. Helaja and Y. Li, *Proc. Natl. Acad. Sci. U. S. A.*, 2023, **120**, e2303564120.
9 (*a*) O. I. Afanasyev, E. Kuchuk, D. L. Usanov and D. Chusov, *Chem. Rev.*, 2019, **119**, 11857–11911; (*b*) S. Caron, R. W. Dugger, S. G. Ruggeri, J. A. Ragan and D. H. B. Ripin, *Chem. Rev.*, 2006, **106**, 2943–2989; (*c*) J. Magano and J. R. Dunetz, *Org. Process Res. Dev.*, 2012, **16**, 1156–1184.
10 (*a*) J. Cossy and D. Belotti, *Org. Lett.*, 2002, **4**, 2557–2559; (*b*) X. Jie, Y. Shang, Z.-N. Chen, X. Zhang, W. Zhuang and W. Su, *Nat. Commun.*, 2018, **9**, 5002; (*c*) S. Paganelli, R. Tassini and O. Piccolo, *ChemistrySelect*, 2022, **7**, e202202393.
11 S. A. Girard, H. Huang, F. Zhou, G.-J. Deng and C.-J. Li, *Org. Chem. Front.*, 2015, **2**, 279–287.
12 S. U. Dighe, F. Juliá, A. Luridiana, J. J. Douglas and D. Leonori, *Nature*, 2020, **584**, 75–81.
13 (*a*) S.-K. Tao, S.-Y. Chen, M.-L. Feng, J.-Q. Xu, M.-L. Yuan, H.-Y. Fu, R.-X. Li, H. Chen, X.-L. Zheng and X.-Q. Yu, *Org. Lett.*, 2022, **24**, 1011–1016; (*b*) J. Hu, R. Ma, J. Hu, X. Liu, X. Liu, H. He, H. Yi and A. Lei, *Green Chem.*, 2024, **26**, 4684–4690.
14 (*a*) J. Corpas, H. P. Caldora, E. M. Di Tommaso, A. C. Hernandez-Perez, O. Turner, L. M. Azofra, A. Ruffoni and D. Leonori, *Nat. Catal.*, 2024, **7**, 593–603; (*b*) J. Kim, S. Kim, G. Choi, G. S. Lee, D. Kim, J. Choi, H. Ihee and S. H. Hong, *Chem. Sci.*, 2020, **12**, 1915–1923.
15 (*a*) W.-C. Lin, T. Yatabe and K. Yamaguchi, *Chem. Lett.*, 2025, **54**, upaf043; (*b*) F. Chen, H. Geng, C. Li, J. Wang, B. Guo, L. Tang and Y.-Y. Yang, *J. Org. Chem.*, 2023, **88**, 15589–15596.
16 A. Lenarda, I. Jain, A. Kaleva, V. Oksanen, S. Heikkinen, R. Koivula, T. Wirtanen, M. Melchionna, T. Hu and J. Helaja, *Green Chem.*, 2026, **28**, 199–212.
17 H. Zhao, H. P. Caldora, O. Turner, J. J. Douglas and D. Leonori, *Angew. Chem., Int. Ed.*, 2022, **61**, e202201870.
18 J. Figueiredo, M. Pereira, M. Freitas and J. Órfão, *Carbon*, 1999, **37**, 1379–1389.
19 W. Guo, L. Yu, L. Tang, Y. Wan and Y. Lin, *Nanomicro Lett.*, 2024, **16**, 125.
20 A. E. Wendlandt and S. S. Stahl, *Angew. Chem., Int. Ed.*, 2015, **54**, 14638–14658.
21 (*a*) G.-F. Han, F. Li, W. Zou, M. Karamad, J.-P. Jeon, S.-W. Kim, S.-J. Kim, Y. Bu, Z. Fu, Y. Lu, S. Siahrostami and J.-B. Baek, *Nat. Commun.*, 2020, **11**, 2209; (*b*) G. Lv, H. Wang, Y. Yang, T. Deng, C. Chen, Y. Zhu and X. Hou, *ACS Catal.*, 2015, **5**, 5636–5646.